Humanity and Science　Journal of the Faculty of Health and Welfare, Prefectural University of Hiroshima　10（1）　27－36　2010

Validation of optimal cut-off frequency using a Butterworth filter in single photon emission computed tomography reconstruction for the target organ: Spatial domain and frequency domain

Hideo ONISHI *1*3　Yuki MATSUTAKE *2
Norikazu MATSUTOMO *3　Hizuru AMIJIMA *4

*1 Department of Communication Sciences and Disorders, Faculty of Health and Welfare, Prefectural University of Hiroshima
*2 Center for Diagnostic Imaging, Kurume University Hospital
*3 Program in Health and Welfare, Graduate School of Comprehensive Scientific Research, Prefectural University of Hiroshima
*4 Department of Nursing, Hyogo University of Health Sciences

Received　7 September 2009
Accepted 17 December 2009

Abstract

In single photon emission computed tomography (SPECT) images, we evaluated cut-off frequency using two methods: spatial domain method (normalized mean square error: NMSE) and frequency domain method (radius direction distribution function in the power spectrum: Pr (n)) and we calculated the optimal cut-off frequency of the Butterworth filter according to the nuclide and collimator used, and the target organ. The optimized cut-off frequencies (Fc) were determined for nuclides of 99m-Tc, 123-I, 201-Tl, and LEHR and LEGP collimators, and compared. The Pr (n) was used to evaluate the SPECT images for frequency domain analysis, and the NMSE method was used for the assessment of images in spatial domain. In the brain phantom for both of these methods of analysis, the optimal Fc varies depending on the nuclide and collimator. Fc in use for 99m-Tc is 0.802 [cycles/cm] with LEHR and 0.656 [cycles/cm] with LEGP. However, those in use for 123-I are 0.656 [cycles/cm] with LEHR. In the myocardial phantom, the appropriate Fc are 0.516 [cycles/cm] with LEHR, and 0.469 [cycles/cm] with LEGP in use of 99m-Tc. We concluded that the cut-off frequency of the Butterworth filter should be changed in reconstructing SPECT images according to the collimator, nuclide and target organs.

Key words : Butterworth filter, optimal cut-off frequency , SPECT image, normalized mean square error , radius direction distribution function

1 Introduction

In recent years, radiological technology has advanced remarkably. The development of radiopharmaceuticals for nuclear medicine techniques and improvement in single photon emission computed tomography (SPECT) instruments have also been marked. Under such circumstances, the need to improve the resolution of SPECT images and to devise a SPECT technique allowing more quantitative evaluation has also increased. Improving the usefulness of SPECT images in making quantitative assessment can be roughly regarded to involve three factors.

The first factor is reconstruction of images. This factor has been discussed for many years as a problem during filtering. Various images can be reconstructed using a combination of preprocessing filters (pre-filters) and reconstruction filters.[1) 2) 3)] The second factor is correction for attenuation and scattering. Methods of correcting for attenuation, known for many years, include those proposed by Sorenson[4) 5)] and Chang.[6) 7)] High-accuracy correction for attenuation is now becoming possible by preparing absorption maps using the transmission method[8) 9) 10)] and CT scanner method.[11) 12)] The problem how to correct for scattering has remained an unresolved issue for many years. However, the recent introduction to the clinic of methods such as the triple energy window method (TEW) [13) 14)] and the transmission dependent method for scatter correction (TDSC)[15)16)17)] has made it possible to achieve satisfactory correction for scattering. The third factor is the partial volume effect. This problem is often seen in low-resolution nuclear medicine images. This is a difficult problem associated with the physical properties of SPECT images.[18)19)20)] If these three factors can be improved, SPECT images with highly accurate quantitative information can be obtained.

Availability of a noise reduction filter in SPECT reconstruction is proved by many clinical studies. The Butterworth Filter is called a Low-pass filter, this filter has two parameters that determine its shape and has the most flexibility in tailoring the properties of the filter by a change of the cut-off frequency particularly, and it is generally adopted in many institutions. In general, this filter is used as a pre processing filter, and used to remove high frequency noise or control it with cut-off frequency. The cut-off frequency of the Butterworth filters determines the amount of smoothing and loss of resolution in the reconstruction image. When we adjust cut-off frequency to low values, reconstruction images were more smoothed and image resolution deteriorates. Determination of cut-off frequency of this filter is decided by subjective sensation like the visual inspection of the physician and technologists. Regarding the cut-off frequency of the Butterworth filter, only qualitative views have been presented in previous studies, and no quantitative discussion of this issue has been made. This paper discusses cut-off frequency from the two methods of spatial domain (normalized mean square error: NMSE) method [21) 22)] and frequency domain (radius direction distribution function in the power spectrum: Pr (n)) method[23)], and we calculated optimal cut-off frequency of the Butterworth filter according to the nuclide and collimator used, and the target organ.

2 Material and Methods

2.1 Equipment

We used a SPECT-2000H-4 4-detector SPECT machine (Hitachi, Tokyo) with a low-energy high resolution (LEHR) collimator with a full width at half maxiam (FWHM) of 7.4 mm and with a low-energy general purpose (LEGP) collimator with a FWHM of 12 mm at brain phantom acquisition and used GCA-901A SPECT machine (Toshiba, Tokyo) with a LEHR collimator with a FWHM of 7.6 mm and with LEGP collimator with a FWHM of 12.5 mm at myocardial phantom.

2.2 Data acquisition and Image processing

2.2.1 Brain phantom study

The brain phantom (Kyoto kagaku, Kyoto) consists of a white matter and a gray matter part, 500 cm^3 and 200 cm^3 in volume, respectively. The phantom is oval-shaped (major axis=20 cm, minor axis=15 cm) with the thickness of 7 cm. The radioactivity of white and gray matter parts were adjusted to 6.43 Bq/ cm^3 and 25.72 Bq/ cm^3, respectively, so that the ratio of the two parts became 1 to 4. This phantom insert was filled with 123-I (159 keV) and 99m-Tc (140 keV) for this study. The SPECT acquisition used a 64 x 64 matrix (1pixel=3.4 mm) and projection data were collected in 64 different positions equally spread over 360 degrees. For the process images a 20 seconds acquisition was performed for each position.

A reference image was acquired to be used to calculate the normalized mean square error (NMSE). Counts were accumulated for 200 seconds at each rotation angle, which was ten times longer than that for the process images. Noise was relatively low in these images and these images served as the gold standard for comparison. SPECT images were reconstructed using a two dimensional Butterworth filter (order 8) and a ramp back-projection filter for the process

images, whereas the reference image used a ramp reconstruction filter only for the high quality images. Nine different filter cut-off frequencies, 0.292, 0.364, 0.437, 0.510, 0.583, 0.656, 0.729, 0.802 and 0.875 [cycles/cm], were applied to reconstruct each of the SPECT images. When the attenuation correction was performed by the Chang method alone, the attenuation coefficient used with 0.12 cm^{-1} in 123-I and 0.1 cm^{-1} in 99m-Tc. We performed the scatter correction using the TEW method.

2.2.2 Myocardial Phantom study

The myocardial phantom (Kyoto Kagaku, Kyoto) used has hepatic and cardiac spaces. The heart insert had a myocardial space of 200 cm^3 with one defect simulating myocardial infarction. The heart insert was filled with 201-Tl (72 keV) and 99m-Tc for this study. The SPECT acquisition used a 64 x 64 matrix (1pixel=5.3 mm) and was over 180° in 6° steps at 30 seconds acquisition per step. A reference image was used by the NMSE method acquisition time at 10 times the same as the brain phantom as was stated previously. Vertical long-axis SPECT images of the entire left ventricle were displayed from the reconstructed transaxial SPECT images by performing coordinate transformation reorientation with an appropriate interpolation.

SPECT images were reconstructed using a two dimensional Butterworth filter (order 8) and a ramp back-projection filter for the process images, whereas the reference image used ramp reconstruction filter only for the high quality images. In this case we used a Butterworth filter in the same way and changed cut-off frequency, 0.187, 0.234, 0.281, 0.328, 0.375, 0.422, 0.469, 0.516 and 0.563 [cycles/cm], applied to reconstruction of each of the SPECT images. Scatter correction used the TEW method. When the attenuation correction was performed by the Chang method alone, the attenuation coefficient used with 0.08 cm^{-1} in 201-Tl and 0.1 cm^{-1} in 99m-Tc.

2.3 Image Assessment

2.3.1 Radius direction distribution function method

A 2-dimensional Fourier transform F (u, v) was made of image f(x, y) as shown in equation (1). Here, u,v are coordinates in Fourier space. We can express two powers of an absolute value of spectral amplitude as power spectrum.

$$F(u,v) = \int_{-\infty}^{\infty}\int_{-\infty}^{\infty} f(x,y)e^{-j2\pi(ux+vy)}dxdy \qquad (1)$$

Radius r is equivalent to cycles per cm when we think about a frequency band in concentric circles in Fourier space (u, v) of the power spectrum. Equation (2) shows the radius direction distribution function: Pr (n) which is an integration of power spectrum intensity in a ring to own width ⊿r in radius.

$$\Pr(n) = \int_0^{2\pi}\int_{n\Delta r}^{(n+1)\Delta r} \left|F(u,v)\right|^2 rdrd\theta \qquad (2)$$

The Pr (n) is obtained from the two-dimensional power spectra of reference and process images, to evaluate the signal spectrum distribution. Pr (n) involves one-dimensional substitution of the two-dimensional signal spectrum of the same frequency (in the direction of the radius vector) from the two-dimensional power spectrum of SPECT images.

2.3.2 N.M.S.E method

Pixel-by-pixel operation is conducted between the reference image, *f(x,y)*, and the processed image, *g(x,y)*. Square errors between the two images are calculated using equation (3).

$$NMSE = \frac{\sum_{i=0}^{x}\sum_{j=0}^{y}(g(i,j)-f(i,j))^2}{\sum_{i=0}^{x}\sum_{j=0}^{y}f(i,j)^2} \qquad (3)$$

The optimum cut-off frequency was obtained by determining the minimum square error at each frequency between the reference image and the process images.

3. Results

3.1 Brain phantom study

Figure 1 shows the 2D power spectral distributions of the images of the brain phantom for a 99m-Tc nuclide as used with the LEHR and LEGP collimators and the corresponding Pr (n) in response to changes in the cut-off frequency of the Butterworth filter. No subjective differences were observed between the reference images and the process images, except when the cut-off frequency for SPECT imaging was 0.437 [cycles/cm]. However, the power spectral distributions showed significant changes in the higher frequency ranges. Of particular importance about figure 1 is that the signal bandwidth in the frequency range of 0.227 to 1.455 [cycles/cm] was wider with the LEHR collimator than with the LEGP collimator. When approaching most closely to the Pr (n) distribution curve of the reference image, the cut-off frequency was 0.656 [cycles/cm] for the LEGP collimator and 0.802 [cycles/cm] for the LEHR collimator.

Figure 2A shows the Pr (n) distributions associated with two different nuclides (99m-Tc and 123-I) used with the LEHR collimator. The differences in Pr (n) distribution

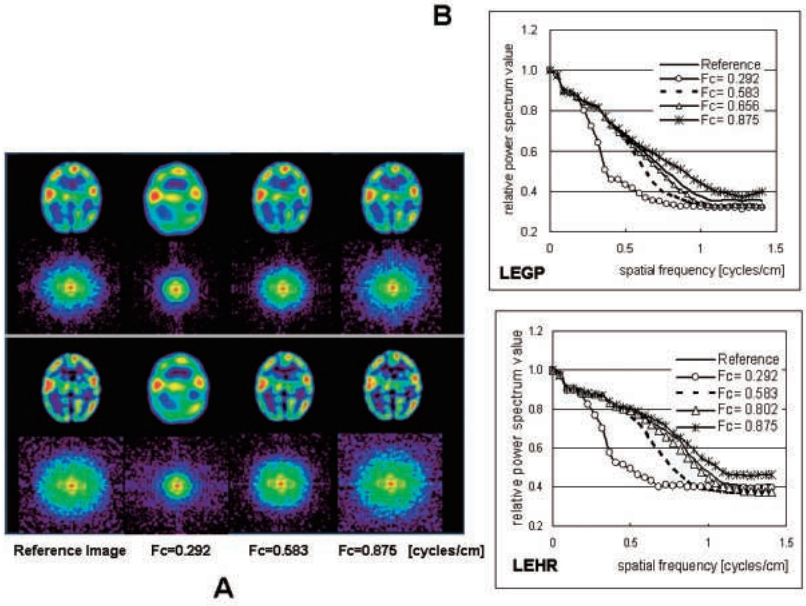

Figure 1 Comparison between different cut-off frequencies for the brain phantom SPECT images, the two-dimensional power spectrum and Pr (n) distribution of collimator systems using the 99m-Tc.

A: The cut-off frequency changes from 0.292 to 0.875 [cycles/cm]. The upper two rows are for the LEGP collimator, and the lower two rows for the LEHR collimator.

B: The Pr (n) of the SPECT process and reference images. The upper row is the LEGP collimator and lower row is the LEHR collimator.

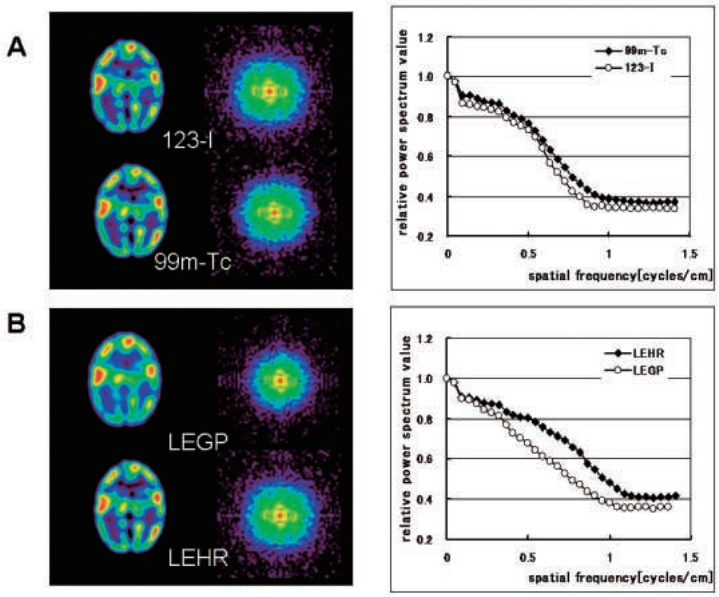

Figure 2 Comparison between Pr (n) in radionuclide and the collimator systems used for the reference image.

A: The left side is reference images and two-dimensional power spectrum for radionuclide (123-I and 99m-Tc) using the LEHR collimator. The right side is Pr (n) distribution of 123-I and 99m-Tc.

B: The left side is reference images and two-dimensional power spectrum for the collimator system (LEGP and LEHR) using 99m-Tc. The right side is Pr (n) distribution of LEGP and LEHR collimator systems.

between the two different nuclides were significant in the frequency range of 0.138 to 1.196 [cycles/cm], and the Pr (n) value in the bandwidth changed from 3.2 % to 14.7 %. Figure 2B shows the frequency distributions of the reference images obtained using two different of collimators (LEHR and LEGP). The signal spectral distribution of the LHER collimator showed higher signal intensity than the LEGP collimator in all frequency ranges and this distribution broadened in the high frequency area.

Figure 3 shows the collimator and nuclide results obtained using the NMSE method, respectively. The four NMSE distribution curves are convex in the downward direction, each with a minimum value. The cut-off frequency at the minimum NMSE value was obtained by a seventh-order polynomial approximation of the NMSE curve (r = 0.93). The cut-off frequency was 0.656 [cycles/cm] for the LEGP collimator used with 99m-Tc, 0.729 [cycles/cm] for the LEHR collimator used with 99m-Tc, 0.583 [cycles/cm] for the LEGP collimator used with 123-I, and 0.656 [cycles/cm] for the LEHR collimator used with 123-I.

3.2 Myocardial Phantom study

Figure 4 shows the 2D power spectral distributions and Pr(n) of the images of the myocardial phantom for 99m-Tc as used with the LEHR and LEGP collimators. Similarly to the above-described case of the brain phantom, the differences in the changes in the cut-off frequency for the LEGP collimator were smaller than for the LEHR. The

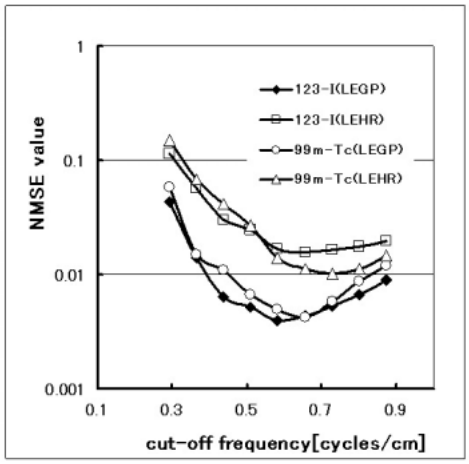

Figure 3 Comparison of the different cut-off frequencies for radionuclide (I-123 and 99m-Tc) and collimator systems (LEGP and LEHR) using NMSE method. NMSE was calculated from each process image.

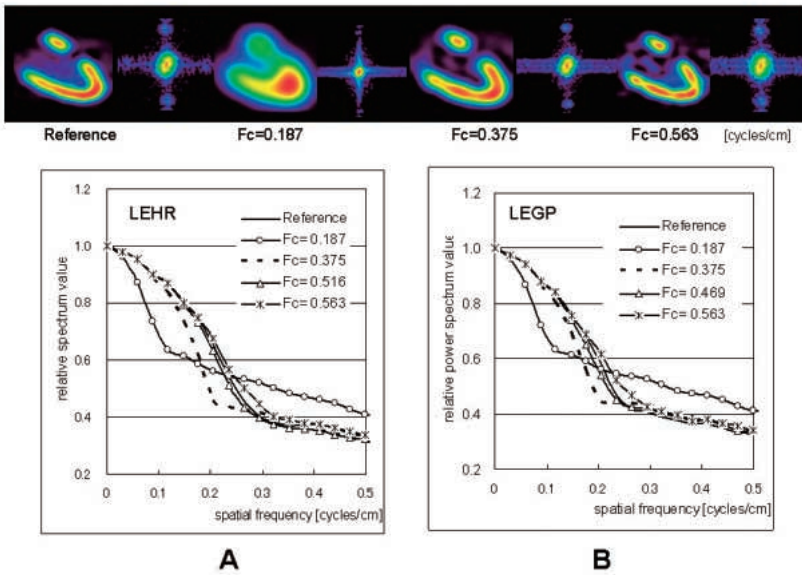

Figure 4 Comparison between different cut-off frequencies for the myocardial phantom SPECT images, the two-dimensional power spectrum and Pr (n) distribution of collimator systems using the 99m-Tc. The Upper row is cut-off frequency changing from 0.187 to 0.563 cycles/cm. A: LEHR collimator　B: LEGP collimator

value of the cut-off frequency was 0.516 [cycles/cm] for the LEHR collimator and 0.469 [cycles/cm] for the LEGP collimator, each showing a distribution close to the Pr (n) of the reference image.

Figure 5 shows the Pr (n) in response to changes in the cut-off frequency for 99m-Tc and 201-Tl used for the LEHR collimator. The cut-off frequency close to that of the reference image was higher with 201-Tl than with 99m-Tc.

Figure 6 shows the collimator-specific NMSE curves for 99m-Tc and 201-Tl. Similarly to the case of the brain phantom, these four curves are convex in the downward direction, each with a minimum value. The cut-off frequency at which the minimum NMSE value was obtained by a seventh-order polynomial approximation of the NMSE curve (r = 0.90) was 0.516 [cycles/cm] for the LEHR collimator used with 99m-Tc, 0.469 [cycles/cm] for the LEHR collimator used with 201-Tl, and 0.469 [cycles/cm] for the LEGP collimator as used with 99m-Tc and 201-Tl.

4 Discussion

Different nuclides and collimators were used to comparatively investigate the optimal cut-off frequencies of the Butterworth filter used primarily for nuclear medical SPECT examinations for cerebral blood flow and cardiac studies. Based on the comparison of the optimal cut-off frequencies in the spatial domain and in the frequency

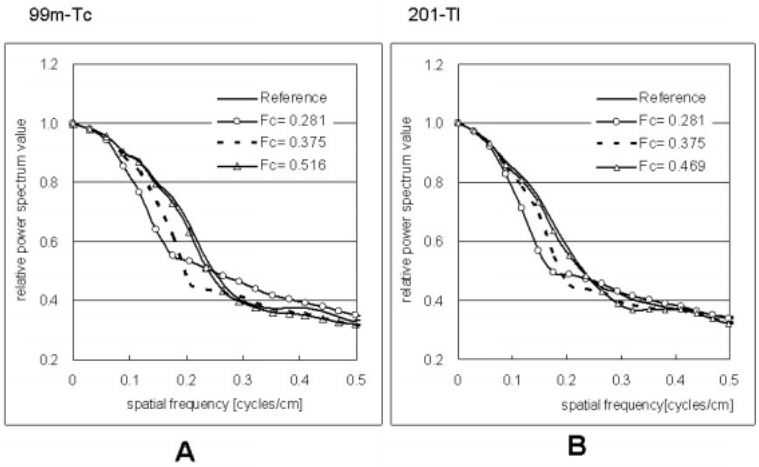

Figure 5 Comparison of the different cut-off frequencies radionuclide (99m-Tc and 201-Tl) and LEHR collimator system used by Pr(n) distribution. Parameter is cut-off frequencies. A: 99m-Tc　B: 201-Tl

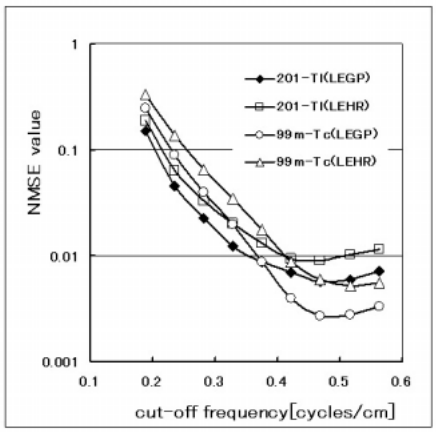

Figure 6 Comparison of the different cut-off frequencies for radionuclide(201-Tl and 99m-Tc) and collimator systems (LEGP and LEHR) using NMSE method. NMSE was calculated from each process image.

domain, the effectiveness and validity of the method of evaluating optimal cut-off frequencies were confirmed. When we performed SPECT image processing in clinical studies, the selection of a correct collimator for the target organ and nuclide to be used is an important step. Collimator selection is made based on the content of the examination and the properties of the nuclide; however, the selection process may be very complicated and involve many priority factors, such as sensitivity and spatial resolution, which may considerably differ from one collimator to another, depending on the purpose of each examination.[24) 25) 26)]

In cerebral blood flow SPECT studies[27)], in particular, counts-dependent cut-off frequencies must be optimally accurate because SPECT values[28)] are directly used for quantification of regional cerebral blood flows (rCBFs). The frequency bandwidth[23)] of an acquired image may vary significantly depending on the collimator used. If an LEHR collimator has a signal dynamic range of "1," those of LEGP and the low-energy high sensitivity (LEHS) collimators will be 0.5 and 0.3, respectively. These differences are reasonably predictable from the Pr (n) distributions for the LEHR and LEGP collimators in figure 1. In other words, these results reveal that the system resolution of the collimator used influences the signal spectrum distribution included in the acquired image. The results also show that target organs differ from each other in their image frequency characteristics.

As shown in figures 1 through 4, the changes in the Pr (n) distributions associated with the collimator used were greater than those attributable to the nuclide used. This indicates that the collimator had a more significant influence on image reconstruction than the nuclide. From the Pr (n) distributions in figures 1 and 2, the signal spectral distributions used by the LEHR collimator were wider than the LEGP collimator, and the system with the LEHR collimator had a wide dynamic range for image frequency characteristics. In the case of the LEHR collimator, the differences between the reference images and the process images increased in response to the changes in the cut-off

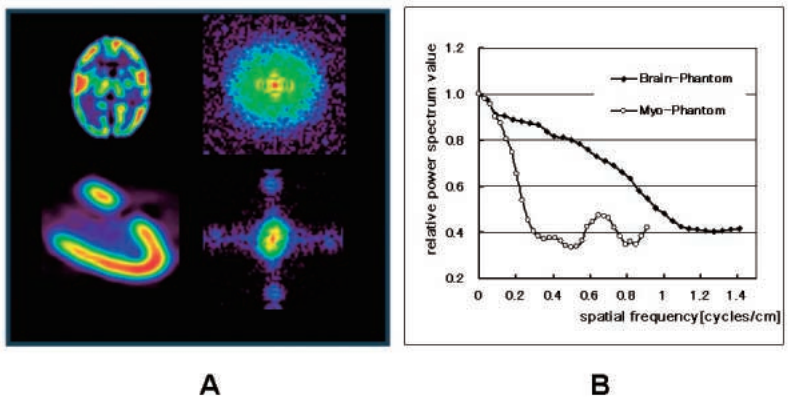

Figure 7 Comparison of the different signal distributions for target organs.
A: The upper row is reference brain phantom images and two-dimensional power spectrum for 99m-Tc radionuclide using the LEHR collimator and the lower row is reference myocardial phantom two-dimensional power spectrum for 99m-Tc radionuclide using the LEHR collimator.
B: The frequency distribution of SPECT images of different organs (brain and myocardial phantom).

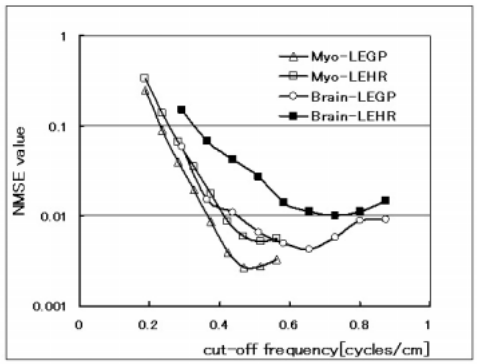

Figure 8 Comparison of the different cut-off frequencies for target organs and collimator systems (LEGP and LEHR) using NMSE method.

frequency. This indicated that the LEHR collimator was more sensitive to filtering than the LEGP collimator.

When the brain phantom and myocardial phantom were acquired using identical 99m-Tc nuclides, the optimal cut-off frequency for the brain phantom was 0.656 [cycles/cm] as used with the LEGP collimator and 0.802 [cycles/cm] as used with the LEHR collimator. The optimal cut-off frequency for the myocardial phantom was 0.469 [cycles/cm] as used with the LEGP collimator and 0.516 [cycles/cm] as used with the LEHR collimator. These results clearly show that an optimal cut-off frequency depends on the target organ. Figure 7 shows the Pr (n) of the images of the brain phantom and the myocardial phantom for 99m-Tc used with the LEHR collimator.

These are no more than the frequency distributions of the images of the phantoms, but show that myocardial image having a relatively simple geometry contained more low-frequency components than high-frequency components. The spectral distribution of the cerebral blood flow image with a relatively complicated geometry extended well into the higher frequency ranges. The image frequency may vary depending on the target organ, as can be seen from these distributions. The cut-off frequency of the Butterworth filtering, which is noise reduction filtering, must be optimally adjusted as appropriate for the target organ.

So far, this study was limited to the evaluation of images in frequency domain. In actual clinical studies, however, physicians depend on visual interpretation for images to arrive at diagnoses. SPECT images were evaluated using the NMSE method, which is supposed to be fully compatible with human vision[25]. The optimal cut-off frequency determined using the NMSE method for the brain phantom used with 99m-Tc was 0.656 [cycles/cm] for the LEGP collimator and 0.729 [cycles/cm] for the LEHR collimator. The optimal cut-off frequency for the myocardial phantom was 0.469 [cycles/cm] for the LEGP collimator and 0.516 [cycles/cm] for the LEHR collimator. These results approximately agree with the optimal cut-off frequencies obtained from the above-described frequency domain.

We obtained results similar to Hambye's study[29] and Kubo's study[30]. As for the LEHR collimator for the brain phantom, however, there was a slight difference between the value obtained from the frequency domain (0.802 [cycles/cm]) and the value obtained from the spatial domain (0.729 [cycles/cm]). The difference is approximately 10% and can be considered to be within tolerable experimental

error limits. Figure 8 shows the NMSE values for the brain phantom and the myocardial phantom. These results suggest that, similarly to the case of the observation in figure 7 above, the cut-off frequency must be optimized as appropriate for the target organ.

5 Conclusion

The optimal cut-off frequency of the Butterworth filter, which is the preprocessing filter for SPECT image processing, was determined and we compared the optimal cut-off frequency in the spatial domain and frequency domain, which confirmed the effectiveness and validity of the method of evaluating optimal cut-off frequencies. In cerebral blood flow SPECT studies using the brain phantom, the optimal cut-off frequency was 0.802 [cycles/cm] for the LEHR collimator used with 99m-Tc, 0.656 [cycles/cm] for the LEGP collimator used with 99m-Tc, 0.656 [cycles/cm] for the LEHR collimator used with 123-I, and 0.583 [cycles/cm] for the LEGP collimator used with 123-I. Therefore, the cut-off frequency must be optimized as appropriate for the collimator and the nuclide to be used. In myocardial perfusion SPECT studies using the myocardial phantom, the optimal cut-off frequency was 0.516 [cycles/cm] for the LEHR collimator used with 99m-Tc, and 0.469 [cycles/cm] for the LEGP collimator used with 99m-Tc. The optimal cut-off frequency was 0.469 [cycles/cm] for the LEHR collimator used with 201-Tl, and 0.469 [cycles/cm] for the LEGP collimator used with 201-Tl.

Additionally, the value of the optimal cut-off frequencies obtained from the frequency domain approximately agreed with those obtained from the spatial domain. The frequency distribution of an image may depend on the acquisition system and nuclide or the scanned target organ. Therefore, the cut-off frequency of the preprocessing filter must be carefully determined.

Reference

1) Ramachandran, G.N. and Laksminarayanan, A.V.: Three-dimensional reconstruction form radiographs an electron micrographs: Application of convolution instead of Fourier transforms. Medical Physics, 68:2236-2240, 1971
2) Boulfelfel, D., Rangayyan, R.M., et al.: Two-dimensional restoration of single photon emission computed tomography image using the Kalman filter. IEEE Transaction on Medical Imaging, 13(1):102-9, 1994
3) Bronnikov, A.V.: A filtering to approach image reconstruction in 3D SPECT. Physics in Medicine and Biology, 45(9), 2639-2651, 2000
4) Sorenson, J.A.: Methods for quantitative measurement of radioactivity in vivo whole-body counting. Instrumentation in Nuclear Medicine, Vol.2(ed. by Heine GJ. and Sorenson JA). New York, Academic Press, 311-348, 1974
5) Walters, T.E., Simon, W., et al.: Attenuation correction in gamma emission computed tomography. Journal of Computer Assisted Tomography, 5:89-94, 1981
6) Chang, L.T.: A method for attenuation correction in radionuclide computed tomography. IEEE Transaction on Nuclear Science, 25:638-643, 1978
7) Larsson, S.A .: Gamma camera emission tomography. Actal Radiology, 3:52-56, 1980
8) Mukai, T., Ishii, Y., et al.: Attenuation and scattering correction of SPECT using transmission CT. Journal of Nuclear Medicine, 23:85-88, 1982
9) Jaszczak, R.J., Gilland, D.R., et al.: Fast transmission CT for determining attenuation maps using a collimated Line Source air-copper lead attenuators and fan Beam Collimation. Journal of Nuclear Medicine, 34:1577-1586, 1993
10) Murase, K., Tanada, S., et al.: Improvement of brain signal photon emission tomography (SPECT) using transmission data acquision in a four-head SPECT scanner. European Journal of Nuclear Medicine, 20:32-38, 1993
11) Fleming, J.S.: A technique for using CT images in attenuation correction and quantification coefficients for use in quantitative single photon emission tomography studies of the thorax. European Journal of Nuclear Medicine, 19:36-40, 1992
12) Takahashi, Y., Murase, K., et al.: Attenuation correction of myocardial SPECT images with X-ray CT: Effect of registration errors between X-ray CT. Annals of Nuclear Medicine, 16: 255-261, 2002
13) Floyd, C.E., Jaszczak, R.J., et al.: Energy and spatial distribution of Multiple order Compton scatter in SPECT: A Monte Carlo simulation. Physics in Medicine and Biology, 29:1217-1230, 1984
14) Ichihara, T., Ogawa, K., et al.: Compton-scatter compensation using the triple energy window method for single and dual isotope SPECT. Journal of Nuclear Medicine, 34:2216-2221, 1993
15) Meikle, S.R., Hutton, B.F., et al.: A transmission dependent method for scatter correction in SPECT. Journal of Nuclear Medicine, 35:360-367, 1994
16) Narita, Y., Eberl, S., et al.: Monte Carlo and

experimental evaluation of accuracy and noise properties of two scatter correction methods for SPECT. Physics in Medicine and Biology, 41:2481-2496, 1996

17) Deloar, H.M., Watabe, H., et al.: Optimization of the Width of the Photopeak Energy Window in the TDCS Technique for Scatter Correction in Quantitative SPECT. IEEE Transaction on Nuclear Science, 51: 625-630, 2004
18) Ogawa, K. and Katsu, H.: Iterative correction method for shift-variant blurring caused by collimator aperture in SPECT. Annals of Nuclear Medicine, 10:33-40, 1996
19) Lalush, D.S. and Tsui, B.M.W.: Mean-Variance Analysis of block iterative reconstruction algorithms modeling 3D detector response in SPECT. IEEE Transaction on Nuclear Science, 45:1280-1287, 1998
20) Yokoi, T., Onishi, H., et al.: Performance evaluation of OSEM reconstruction algorithm incorporating three-dimensional distance-dependent resolution compensation for brain SPECT: A simulation study. Annals of Nuclear Medicine, 16(1): 11-18, 2003
21) Penny, B.C., King, M.A., et al.: Constrained least-squares restoration of nuclear medicine images: selecting the coarseness function. Medical Physics, 14:849-858, 1987
22) King, M.A., Glick, S.J., et al.: Iterative visual optimization of SPECT pre-reconstruction filtering. Journal of Nuclear Medicine, 28:1192-1198, 1987
23) Onishi, H., Takahashi, M., et al.: Evaluation of SPECT image using a textural analysis. Japanese Journal of Radiological Technology, 51:710-716, 1995 [in Japanese]
24) Bronnikov, A.V.: A filtering to approach image reconstruction in 3D SPECT. Physics in Medicine and Biology, 45(9), 2639-2651, 2000
25) Sankaran, S., Frey, E.C., et al.: Optimum compensation method and filter cutoff frequency in myocardial SPECT: a human observer study. Journal of Nuclear Medicine, 43:432-438, 2002
26) Onishi, H., Ota, T., et al.: Two optimal pre-filter cutoff frequencies needed fore SPECT images of myocardial perfusion in a one-day protocol. Journal of Nuclear Medicine Technology, 25(4):256-260, 1997
27) Kotzki, P.O., Mariano-Goulart, D., et al.: Optimum tomographic reconstruction parameters for HMPAO brain SPET imaging: practical approach based on subjective and objective indexes. European Journal of Nuclear Medicine, 22(7):671-677, 1995
28) Onishi, H., Tsuji, A., et al.: Quantification of cerebral blood flow using 123-I-IMP SPECT: A new method of estimating the input function from brain dynamic data. Kakuigaku, 36:121-129, 1999 [in Japanese]
29) Hambye, A.S., Vervaet, A., et al.: Variability of left ventricular ejection fraction and volumes with quantitative gated SPECT: influence of algorithm, pixel size and reconstruction parameters in small and normal-sized hearts. European Journal of Nuclear Medicine, 31:1606-1613, 2004
30) Kubo, N., Mabuchi, M., et al.: Accuracy and reproducibility of left ventricular function from quantitative, gated, single photon emission computed tomography using dynamic myocardial phantoms: effect of pre-reconstruction filters. Nuclear Medicine, Communications, 23:529-536, 2002

人間と科学　県立広島大学保健福祉学部誌　10（1）　27 － 36　2010

SPECT 画像再構成時における Butterworth Filter を用いた標的臓器の最適遮断周波数の実空間と周波数空間での評価

大西　英雄＊1＊3　松竹　裕紀＊2　松友　紀和＊3　網島　ひづる＊4

＊1 県立広島大学保健福祉学部　コミュニケーション障害学科
＊2 久留米大学病院　画像診断センター
＊3 県立広島大学大学院総合学術研究科　保健福祉学専攻
＊4 兵庫医療大学　看護学部

2009 年　9 月　7 日受付
2009 年 12 月 17 日受理

抄録

我々は，脳ファントム及び心臓ファントムで周波数空間と実空間の評価で SPECT 画像における使用核種，コリメータ及び標的臓器の Butterworth フィルタの最適遮断周波数の算出を試みた。周波数空間での評価は動径強度分布関数（Pr（n））を用い，実空間での評価は NMSE 法を用いた。脳ファントムでは核種として 99m-Tc と 123-I を用い，心臓ファントムでは 99m-Tc 及び 201-Tl を使用した。また，コリメータは LEHR 及び LEGP を使用した。脳ファントムでは 99m-Tc における最適遮断周波数は，LEHR で 0.802 [cycles/cm], LEGP で 0.656 [cycles/cm] と変化した。しかし 123-I では LEHR で 0.656 [cycles/cm]であった。心臓ファントムでは 99m-Tc で LEHR は 0.516 [cycles/cm], LEGP で 0.469 [cycles/cm]と変化した。また，同様に 201-Tl でも異なった遮断周波数が算出された。この結果から，SPECT 画像再構成時での Butterworth フィルタの遮断周波数は，使用核種，コリメータ，標的臓器により変化させなければならない。

キーワード：Butterworth フィルタ，最適遮断周波数，SPECT 画像，NMSE 法，動径強度分布関数